Growth kinetics of solidstatereacted FeZr multilayer films

A. Paesano Jr., S. R. Teixeira, and L. Amaral

Citation: Journal of Applied Physics **70**, 4870 (1991); doi: 10.1063/1.349029
View online: http://dx.doi.org/10.1063/1.349029
View Table of Contents: http://scitation.aip.org/content/aip/journal/jap/70/9?ver=pdfcov
Published by the AIP Publishing

Growth kinetics of solid-state-reacted Fe-Zr multilayer films

A. Paesano, Jr., S. R. Teixeira, and L. Amaral
Instituto de Fisica, Universidade Federal do Rio Grande do Sul, 91500 Porto Alegre, Rio Grande do Sul, Brazil

(Received 10 June 1991; accepted for publication 22 July 1991)

Multilayers of $Fe_{0.33}Zr_{0.67}$, prepared by electron beam evaporation, have been characterized by conversion electron Mössbauer spectroscopy, Rutherford backscattering spectroscopy, and x-ray diffraction. Two phases, one amorphous and another crystalline ($FeZr_3$), occur by solid-state reaction. For temperatures of 350 and 500 °C and annealing times ranging from 10 min to 72 h the growth rates of both phases had been obtained. From these results we suggest a model to describe the phase growth kinetics of the amorphous-crystalline $Fe_{0.33}Zr_{0.67}$ multilayer thin film.

I. INTRODUCTION

Since it was established by Schwarz and Johnson[1] that amorphous phases can be obtained by solid-state reaction in multilayer thin films, this process has been the subject of considerable investigation, not only as a new method of forming amorphous alloys, but also in order to get new insights into the underlying kinetic and thermodynamic aspects of amorphous states of matter.

Among other systems, the iron-zirconium couple was reported in some studies. The first one due to Clemens and Suchoski[2] describes the partial amorphization of a multilayered film of average composition $Fe_{61}Zr_{39}$ by annealing at 623 K for 2 h.

Amorphized films with concentration of 50 at. % Fe have also been obtained by Krebs *et al.*[3] using solid-state reactions and co-sputtering processes. They showed that there are differences in the as-prepared samples according to the method of amorphization. However, despite the different starting point, after additional annealing, the sputtered film reaches the same two-separated amorphous phases observed in the reacted film. This two-phase separation could be explained as a result of two local minima in the free-energy diagram. In another study,[4] also with overall composition in the middle of the concentration range, using *in situ* x-ray diffraction and magnetization measurements it was observed amorphization with two clearly different diffusion mechanisms. Anomalous x-ray scattering experiments were done to compare,[5,6] in more detail, an amorphous Fe-Zr system prepared over wider concentration ranges using sputtering, solid-state reaction, and melt-spinning amorphization methods. As the fastest cooling rate occurs in a sputtered process, a larger amorphization range ($20 < x < 93$ at. % Fe) is observed, while there is a limit of range achievable by the two other techniques, $20 < x < 43$ and $89 < x < 91$ at. % Fe for melt-spun ribbons and $45 < x < 55$ at. % Fe for the solid-state reaction.

Another study, at the $Fe_{61}Zr_{39}$ concentration, was done by Williamson and Clemens,[7] with magnetron sputtered and *e*-beam evaporated multilayer samples. From conversion electron Mössbauer results it was found a complete formation of amorphous films when the number of monolayers of each constituent is lower than ten. This amorphous phase is paramagnetic, at room temperature, and the Mössbauer parameters are similar to alloys prepared by melt spinning, sputtering, and *e*-beam evaporation. Furthermore, noticeable differences in the x-ray diffratogram are again reported.

On the other hand, a lot of theoretical approaches for multiphase layer growth have been presented in the literature.[8–17] Considering the influence of interfacial reaction barriers Gösele and Tu[15] have pointed out large differences between thin films and bulk materials. While in the latter the interdiffusion produces simultaneously several intermetallic compounds, a sequential nucleation and growth of compounds have usually been observed in thin films. More recently it was also investigated by them[17] whether this concept can also be applied when the first growing phase is a metastable amorphous alloy.

However, a more close interplay between these theorectical predictions and experimental results mentioned above seems to be difficult, mainly because the usual x-ray and Rutheford backscattering spectroscopy technique used to identify phase formations, often do not permit a clear quantification of the growth of these phases. In particular, this is more evident for the solid-state reaction of multilayered thin films where the grain size of the crystalline phase, if it occurs, can be sufficiently small to be not detected by an x ray. Therefore, to gain new informations in the solid reaction of Fe-Zr multilayers it is interesting to use complementary techniques of analysis, preferably local techniques.

In this sense, we studied a Fe_xZr_{1-x} thin-film multilayered system using Mössbauer spectroscopy as well as Rutherford backscattering spectroscopy and x-ray diffractometry. Our previous study on the $x = 0.67$ and $x = 0.50$ concentrations[18] established that only an amorphous phase is obtained during solid-state reaction. This work reports on the results of the Zr-rich concentration. Unlike the Fe-rich side, the system at the concentration of $x = 0.33$ displays the same amorphous phase but in competition with a new one, the crystalline $FeZr_3$. For temperatures of 350 and 500 °C and annealing times ranging from 10 min to 72 h, the growing rates of both phases had been obtained. Besides this experimental systematic for the sequence of phase formation, we propose some modifications of the approach due to Gösele and Tu[15] in order to derive new expressions for the growth kinetics of this amorphous-crystalline Fe-Zr system.

 0021-8979/91/094870-07$03.00

II. EXPERIMENTAL DETAILS

The Fe-Zr multilayer samples were prepared by sequential evaporation on oxidized silicon substrate using a dual *e*-gun system (Balzers UMS 500P) in an ultrahigh-vacuum chamber with a base pressure of 1×10^{-8} mbar at room temperature. For an overall composition of $Fe_{0.33}Zr_{0.67}$ the multilayer films were constructed by a superposition of five bilayers of 50-Å Fe and 200-Å Zr. All the thermal annealings were performed under a vacuum of better than 2×10^{-7} mbar.

Rutherford backscattering (RBS) analysis was done using an alpha particle beam of 760 keV with incident and scattering angle of 0° and 160°, respectively. The overall resolution of the RBS spectrometer was 13 keV. The x-ray diffractograms were obtained using the Cu K_α radiation in a conventional Siemens diffractometer.

Conversion electron Mössbauer spectroscopy (CEMS) measurements were obtained in a backscattering geometry, using a source of ^{57}Co in a rhodium matrix. All the CEMS spectra were measured at room temperature using a conventional constant acceleration Mössbauer setup.

III. RESULTS

A. Rutherford backscattering

The RBS spectrum of the as-deposited sample [Fig. 1(a)] shows a well-defined multilayered structure. From the five Zr layers the uppermost three are distinguishable on the high-energy side of the spectrum. From the low-energy side, three of the five Fe layers can be counted. The two higher peaks appearing at the middle part of the spectrum correspond to the superposition of the last two peaks of Zr with the two uppermost external peaks of the Fe.

A typical RBS spectrum for the annealed samples at 350 °C is shown in Fig. 1(b) where a reaction between the Fe and Zr layers occurs, although the multilayer structure still remains. The more pronounced modifications occur in the low-energy side, as indeed is expected, because the iron is the dominant moving species.[19] Figure (1c), shows the characteristic RBS spectrum for the samples annealed at 500 °C. Further decreases in the multilayered structure are then observed.

B. X-ray analysis

A typical x-ray diffractogram of the as-deposited samples is shown in Fig. 2(a) where the peaks corresponding to Fe(110), Zr(100), Zr(101), and Zr(002) can be identified.

Figure 2(b) displays the x-ray diffractogram corresponding to the sample annealed at 350 °C during 24 h. We observe the complete disappearance of the Fe(110) peak. The annealing of the sample at 500 °C for 3 h shows the appearance of a new phase. Following the established phase diagram[20] for the Fe-Zr system, this phase can be assigned as the $FeZr_3$[21] crystalline compound. The more pronounced reflections of x-ray spectrum are indicated on the Fig. 2(c). The diffraction lines of this crystalline phase also appear in diffractograms of samples annealed at 350 °C for times as long as 72 h.

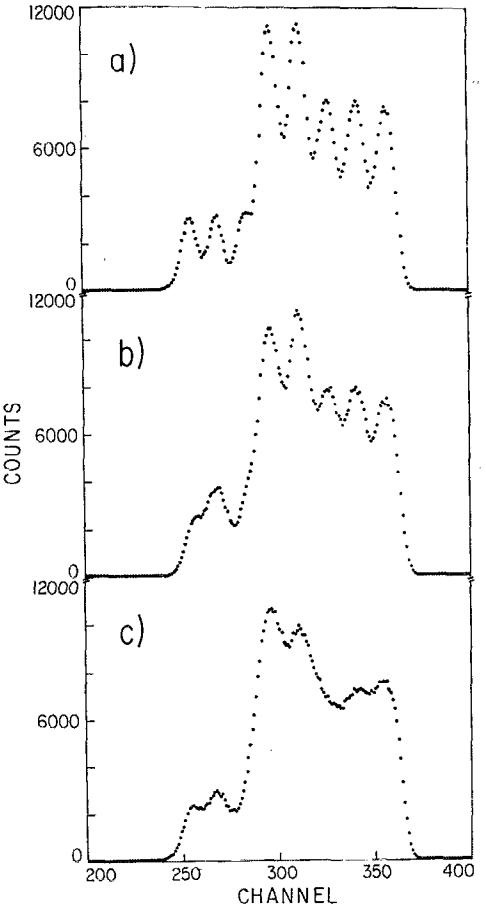

FIG. 1. RBS spectra for the $Fe_{0.33}Zr_{0.67}$ multilayer film: (a) as-deposited, (b) after annealing at 350 °C during 24 h, (c) after annealing at 500 °C during 3 h.

C. Mössbauer spectroscopy

The Mössbauer spectra of the as-deposited and reacted samples are shown in Figs. 3, 4, and 5. The as-deposited spectra [Fig. 3(a)] show a predominant sextet corresponding to metallic iron. Figure 3(b) shows the spectrum of the sample annealed during 10 min at 350 °C. Besides the lines of iron sextet it is possible to see superimposed resonances corresponding to reacted phases.

Figures 4 and 5 display the spectra of the samples annealed during 1 h and 72 h, at 350 °C, and during 20 min and 3 h, at 500 °C respectively. From these spectra we can see that there is no more unreacted metallic iron, but only two paramagnetic superimposed spectra. Then, the measures were taken within a smaller velocity range in order to get a better resolution of the central part of the spectrum.

A good fit can be obtained by taking two quadrupole splittings. The first subspectrum (site A) corresponds to the typical amorphous phase described in the literature,[22–30] while the second one (site B) identifies the $FeZr_3$ crystalline intermetallic compound.[20,23,24,31,32] Table I shows the obtained hyperfine parameters and the relative

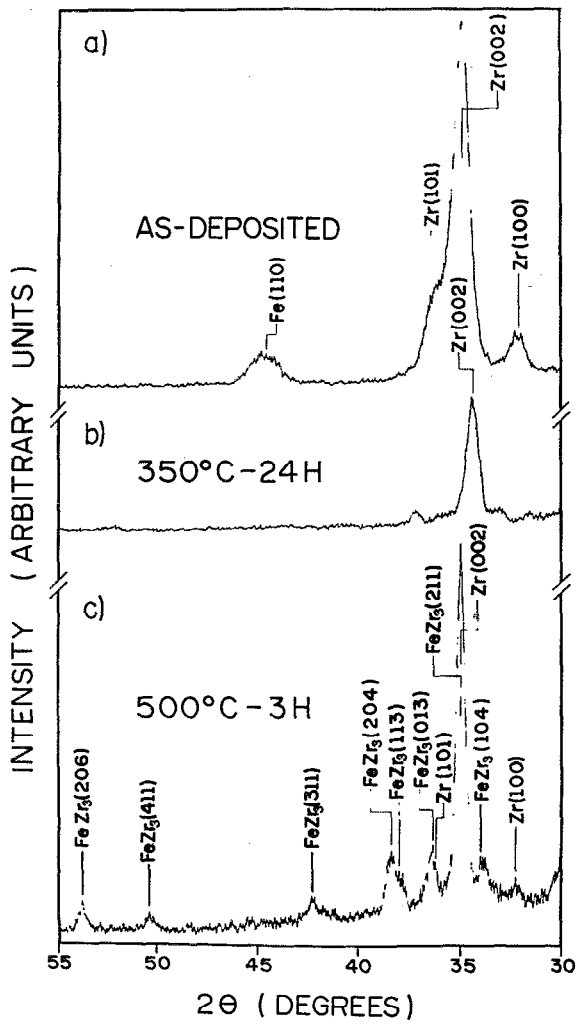

FIG. 2. X-ray diffractograms for the $Fe_{0.33}Zr_{0.67}$ film: (a) as-deposited, (b) after annealing at 350 °C during 24 h, (c) after annealing at 500 °C during 3 h.

fractions of the amorphous phase are plotted in Figs. 6(a) and 6(b) for 350 and 500 °C.

These results, i.e., the increase of the amorphous phase fraction at 350 °C [Fig. 6(a)] and the decrease at 500 °C [Fig. 6(b)] will be discussed in the next section.

IV. DISCUSSION

The x-ray and Mössbauer results indicate that we have an amorphous phase (site A) and a crystalline intermetallic compound $FeZr_3$ (site B), after the solid-state reaction of $Fe_{0.33}Zr_{0.67}$ multilayers. This reaction, which occurs in both temperatures (350 and 500 °C), may be represented in a Gibbs free energy versus composition diagram for the Fe-Zr system, as schematically drawn in Fig. 7. The pathway followed by the reaction is the OB line segment. Initially, the sample has only unreacted material. The Gibbs free energy of the as-deposited $Fe_{0.33}Zr_{0.67}$ multilayer is represented by the O point. As the annealing proceeds and the diffusion process goes on, the free energy of the system decreases by the formation of the two phases, *a*-FeZr and

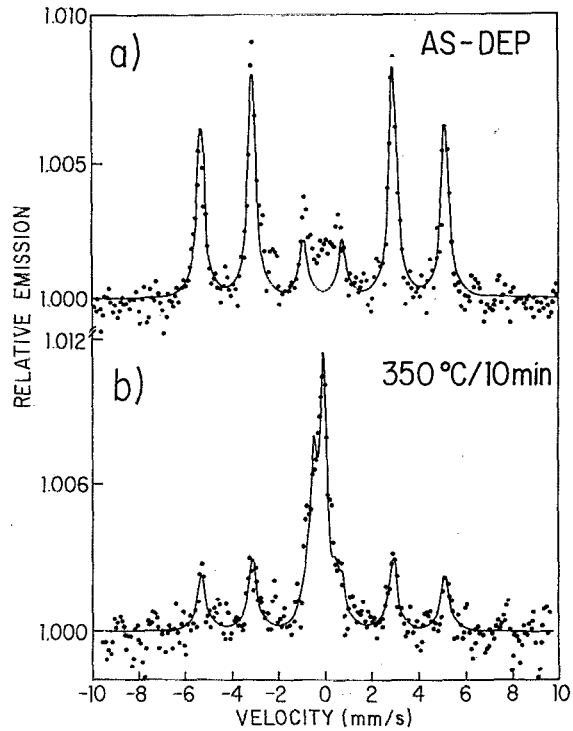

FIG. 3. CEMS spectra measured at room temperature for the $Fe_{0.33}Zr_{0.67}$ film: (a) as-deposited, (b) after annealing at 350 °C during 10 min.

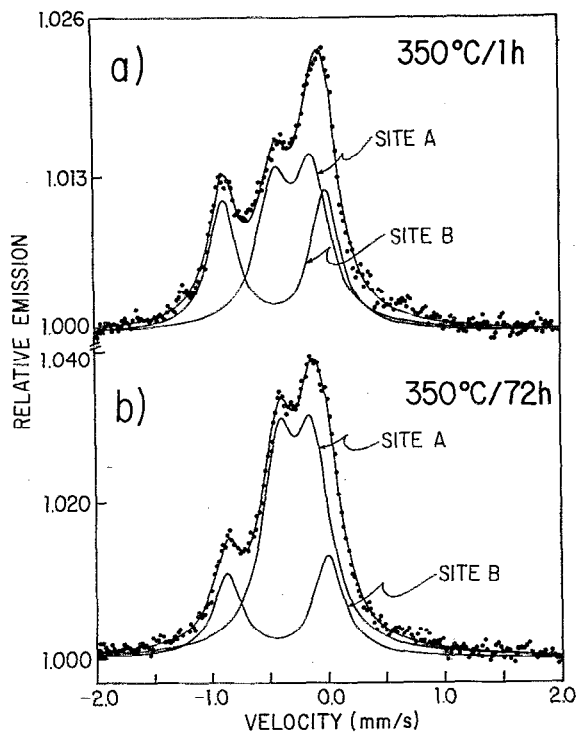

FIG. 4. CEMS spectra measured at room temperature for the reacted samples: (a) after annealing at 350 °C during 1 h, (b) after annealing at 350 °C during 72 h.

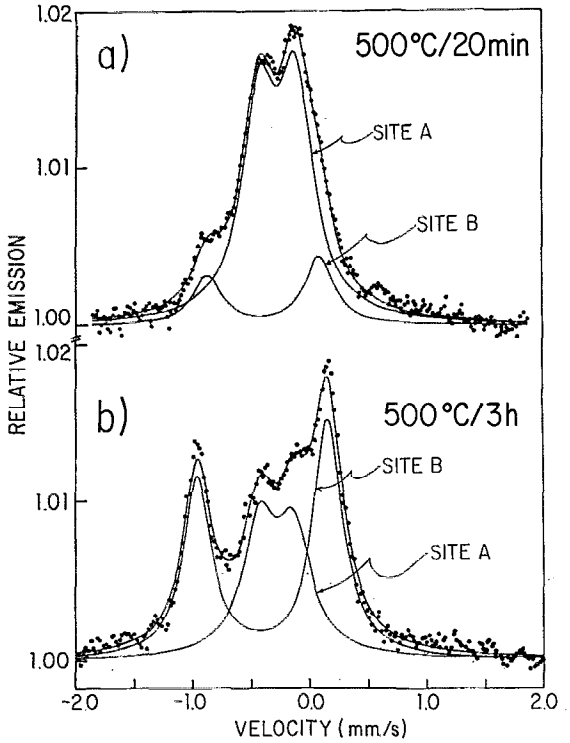

FIG. 5. CEMS spectra measured at room temperature for the reacted samples: (a) after annealing at 500 °C during 20 min, (b) after annealing at 500 °C during 3 h.

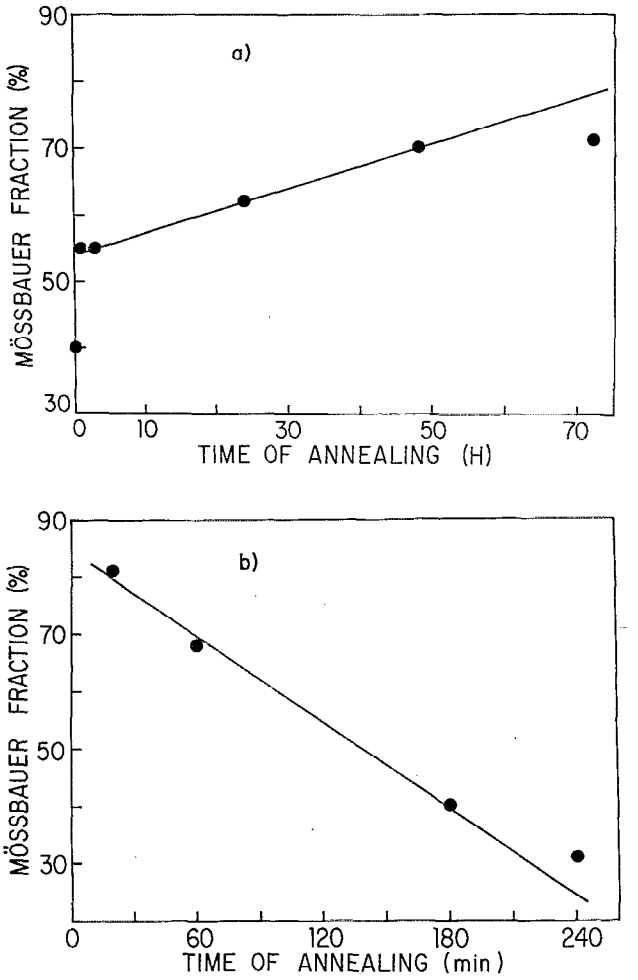

FIG. 6. Mössbauer relative area fraction for the amorphous phase as a function of the annealing time: (a) at 350 °C, (b) at 500 °C.

c-$FeZr_3$. As stated by the common tangent rule, this process occurs until all the elemental iron and zirconium have reacted, when the system reaches point B in the free-energy diagram. At this point, the amorphous portion of the sample has concentration C_1^{eq} and the crystal layers have also a homogeneous concentration C_2^{eq}. Here C_1^{eq} and C_2^{eq} represent the equilibrium concentrations between the crystal ($FeZr_3$) and the amorphous phases. Point B is a metastable equilibrium state where the relative quantities of crystal and amorphous phases can be estimated by the lever's rule.[33]

The first stage of the process already shows two reacted phases [see CEMS spectrum of 350 °C/10 min in Fig. 3(b)] but the elemental iron and zirconium are still present. Assuming that the reactions occur only at interfaces, shown in Fig. 8(a) is a profile of iron concentration as a function of position in a schematic representation of both phases between Fe and Zr elemental layers. These two phases (a-FeZr and c-$FeZr_3$) compete among themselves, growing or shrinking between the saturated phases (α-Fe and α-Zr). This picture, probably, in the beginning of the process, is the same at 500 °C. With a similar concentration profile scheme, Gösele and Tu[15] derive a model for the kinetic of growth of competitive phases. In this model, a critical thickness (X^{crit}) of the first formed phase, eventually an amorphous phase,[17] is established as a condition for the growth of a second nucleated crystalline phase.

TABLE I. Mössbauer parameters used to fit the CEMS data. The isomer shift refers to the metallic iron.

	Site A		Site B		
Annealing time	IS (mm/s)	E_Q (mm/s)	IS (mm/s)	E_Q (mm/s)	Temp.
10 min	−0.16	0.32	−0.23	0.88	350 °C
1 h	−0.16	0.32	−0.32	0.88	350 °C
3 h	−0.15	0.30	−0.31	0.90	350 °C
24 h	−0.16	0.28	−0.32	0.86	350 °C
48 h	−0.15	0.32	−0.28	1.06	350 °C
72 h	−0.16	0.30	−0.32	0.88	350 °C
20 min	−0.16	0.32	−0.29	0.96	500 °C
1 h	−0.17	0.32	−0.28	0.98	500 °C
3 h	−0.17	0.30	−0.29	1.12	500 °C
4 h	−0.19	0.28	−0.30	1.12	500 °C

The equations of phase growth are given by:

$$\frac{dX_\beta}{dt} = G_\beta J_\beta^A - G_{\beta\gamma} J_\gamma^A, \tag{1}$$

$$\frac{dX_\gamma}{dt} = G_\gamma J_\gamma^A - G_{\gamma\beta} J_\beta^A. \tag{2}$$

Here, γ is the first formed phase that must overcome the critical thickness X^{crit}. The β is the second formed phase

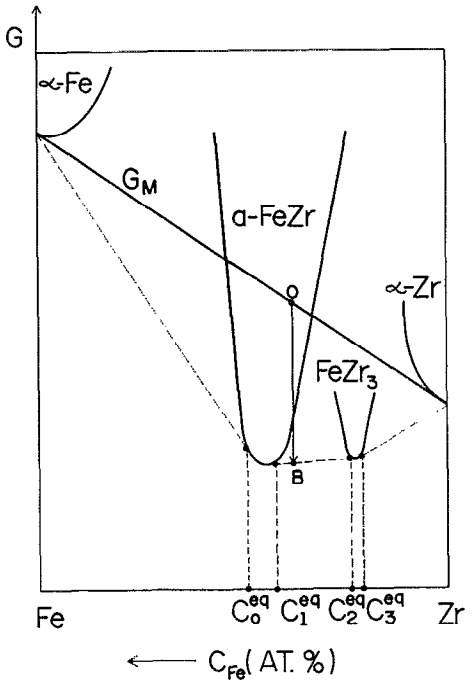

FIG. 7. Gibbs free-energy G as a function of the Fe concentration in the Fe-Zr system. G_M refers to the free-energy of the multilayer and the C^{eq}'s indicate the range of equilibrium concentrations between iron and amorphous phase (C_0^{eq}), amorphous and crystal phase (C_1^{eq} and C_2^{eq}), crystal and zirconium (C_3^{eq}).

that can nucleate, but only grows if X exceeds X^{crit}, at least, while any of two supply elements are not exhausted. J_γ^A and J_β^A are the fluxes of A atoms in the γ and β phases, respectively. The quantities G_β, G_γ, $G_{\beta\gamma}$, and $G_{\gamma\beta}$ are functions of the composition at the interfaces.

This analysis (#3 of Ref. 15) can be strictly applied to describe the first stage of the reaction in our Fe-Zr multilayers. Nevertheless, for longer annealing times the iron is exhausted although zirconium is not. In some instances the two adjacent amorphous layers touch themselves forming a single one. The entire layer has, in principle, a symmetrical

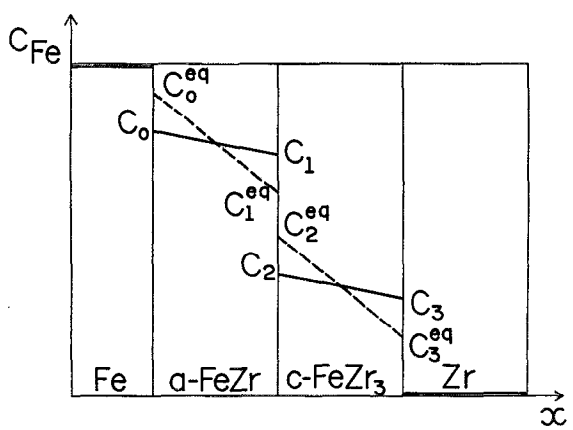

FIG. 8. Schematic of concentration profile of Fe atoms as a function of position, in the beginning of the solid state reaction ($t = 10$ min).

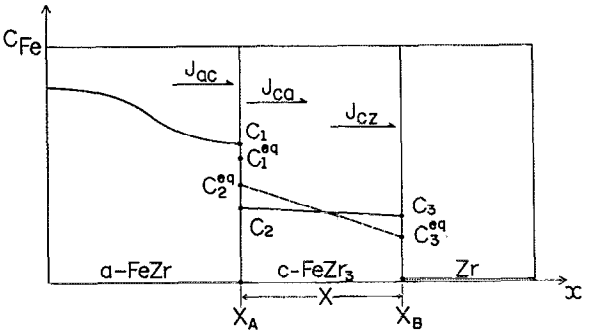

FIG. 9. Schematic of concentration profile after the complete exhaustion of the Fe layer.

iron concentration profile, not constant along it. Figure 9 shows a schematic concentration profile of Fe atoms in some portion of the film where there now appears only half of the amorphous layer. Since the iron is exhausted, a new regime of diffusion is established. In this case, the predictions of approach of Gösele and Tu[15,17] cannot take into account our results. However, with some modifications we are able to describe the measured area fractions [Figs. 6(a) and 6(b)].

To summarize, we have now a compound layer (c-$FeZr_3$) growing or shrinking between another layer (a-FeZr) (with variable profile concentration) and a homogeneous phase of α-Zr (see Fig. 9).

The equations for the change of position of the two interfaces can be rewritten as:

$$(C_1 - C_2)\frac{dX_A}{dt} = J_{ac} - J_{ca}, \tag{3}$$

where now $J_{ac} = -\tilde{D}_a(dC_a/dx)_A$ and $J_{ca} = -\tilde{D}_c(dC_c/dx)_A$; $\tilde{D}_a$ and $\tilde{D}_c$ refer to the interdiffusivity coefficients in amorphous and crystal phases, respectively, and

$$C_3\frac{dX_B}{dt} = J_{cz}, \tag{4}$$

where $J_{cz} = -\tilde{D}_c(dC_c/dx)_B$.

J_{ac} and J_{ca} (see Fig. 9) are the fluxes at interface A, from amorphous phase and to crystal phase, respectively. J_{cz} is the flux from crystal phase at interface B. X_A and X_B are the positions of the amorphous-crystal and crystal-zirconium interfaces, respectively.

The difference relative to the result of Gösele and Tu [Eqs. (1) and (2) of Ref. 15] is the first term in the right-hand side of Eq. (3), which is identified with the flux J_{ac} from the amorphous phase at interface A. It arises from the nonuniform iron concentration profile in the amorphous phase.

If the barriers of diffusion at each interface are considered and using usual definitions,[9,15] the fluxes are given by

$$J_{ac} = K_{ac}(C_1 - C_1^{eq}), \tag{5}$$

$$J_{ca} = -K_{ca}(C_2 - C_2^{eq}), \tag{6}$$

$$J_{cz}=K_{cz}(C_3-C_3^{eq}), \tag{7}$$

where K_{ac}, K_{ca}, and K_{cz} are the reaction constants at interfaces.

Assuming a steady-state diffusion in the intermediary layer we have

$$J=J_{ca}=J_{cz}=\tilde{D}_c(C_2-C_3)/X. \tag{8}$$

Calculating the change of layer with time by using Eqs. (3), (4), and (8), results in

$$\frac{dX}{dt}=\frac{dX_B}{dt}-\frac{dX_A}{dt}=GJ-\frac{J_{ac}}{(C_1-C_2)}, \tag{9}$$

where

$$G=\frac{1}{C_3}+\frac{1}{(C_1-C_2)},$$

or

$$\frac{dX}{dt}=\frac{J}{C_3}+\frac{(J-J_{ac})}{(C_1-C_2)}. \tag{10}$$

The flux J, by combining Eqs. (6), (7), and (8), can be rewritten as[15]

$$J=\Delta C^{eq}\frac{K}{(1+XK/\tilde{D}_c)}, \tag{11}$$

where

$$\Delta C^{eq}=C_2^{eq}-C_3^{eq}, \quad \frac{1}{K}=\frac{1}{K_{ca}}+\frac{1}{K_{cz}}.$$

The term $1/K$ is related to the magnitude of barrier against the diffusion through the interfaces of the crystal layer. G, on the other hand, is an interface compositional dependent (through C_1, C_2, and C_3) and, therefore, must vary with time.

Comparing J_{ac} with J [Eqs. (3) and (10)], three cases may be analyzed:

$$\text{(i)}\ \frac{J_{ac}}{J}<1. \tag{12}$$

When this happens, $dX_a/dt<0$ and $dX/dt>0$, which means the amorphous phase shrinks and the crystalline phase grows at the expense of that phase;

$$\text{(ii)}\ 1\leqslant\frac{J_{ac}}{J}\leqslant G(C_1-C_2). \tag{13}$$

Now, both phases can grow. In each limit of the unequality each phase has null growth;

$$\text{(iii)}\ \frac{J_{ac}}{J}>G(C_1-C_2). \tag{14}$$

In this case, the situation is such that the intermediary phase (crystal) shrinks and the amorphous layer can grow at its expense. This interesting possibility is not foreseen when the amorphous is constrained to be a saturated phase. All the possibilities are schematically indicated in Fig. 10. It must be reinforced that when one phase grows, the other not necessarily shrinks but when a phase shrinks the other certainly grows.

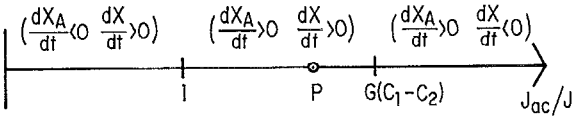

FIG. 10. Schematic of various growth and shrinkage regimes for the competing amorphous and crystalline phases.

Then, looking at the graphics in Figs. 6(a) and 6(b) we can see, in both temperatures, the variation of the Mössbauer fraction (F_a) of the amorphous phase. As we are dealing with fractions it is clear that

$$\frac{dF_a}{dt}=\frac{-dF_c}{dt}, \tag{15}$$

where F_c is the Mössbauer fraction of crystal phase.

If we can relate an average concentration of iron atoms to each of the two phases present in the Mössbauer spectra, the fraction of amorphous phase is given by

$$F_a=\frac{f_aC_aX_A}{(f_aC_aX_A+f_cC_cX)}, \tag{16}$$

where C_a, C_c, f_a, and f_c are the average concentrations and the f factors of the amorphous and the crystal phases, respectively.

Taking the time derivative of F_a, we are left with

$$\frac{dF_a}{dt}=\frac{1}{(X_A+X_C)^2}\left(X_C\frac{dX_A}{dt}-X_A\frac{dX_C}{dt}\right), \tag{17}$$

where

$$X_C=\left(\frac{f_cC_c}{f_aC_a}\right)X.$$

Using Eqs. (3), (9), and (17), it is straightforward to show that when $dF_a/dt\geqslant 0$, then

$$(a)\ \frac{J_{ac}}{J}\geqslant qG(C_1-C_2)+(1-q), \tag{18}$$

where

$$q=\frac{X_A}{X_B}<1,$$

otherwise

$$(b)\ \frac{J_{ac}}{J}<qG(C_1-C_2)+(1-q), \tag{19}$$

when $dF_a/dt<0$.

As $G(C_1-C_2)$ is greater than unity, the value of the right side of the above unequalities is constrained in the interval $[1, G(C_1-C_2)]$ and is represented by the P point in the axis of Fig. 10. Above this point, the ratio between J_{ac} and J implies an increase of the Mössbauer fraction of the amorphous subspectrum. Below the P point, crystal phase has a positive fraction time rate (i.e., $dF_c/dt>0$).

At 350 °C, as is shown in Fig. 6(a), the amorphous phase thickness grows more than the crystalline phase thickness [i.e., $(1/X_A)(dX_A/dt) > (1/X)(dX/dt)$] until 50 h of annealing, when it attains 70% of the Mössbauer spectral area. During this time interval, the crystalline phase can grow or not, or shrink. More annealing time ($\sim$72 h) does not substantially change the relation between Mössbauer areas, showing that the system has reached the thermodynamical metastable point B (Fig. 7). In this state, Zr is also totally consumed and the two phases have homogeneous concentrations. Unfortunately, it is not possible to observe the consumation of Zr by x-ray analysis, due to the superposition of its reflection lines with those of $FeZr_3$ present in the diffractograms.

At 500 °C, the relation among thickness growths is inverted and the crystal grows more than the amorphous phase. As expected, the process is faster than that at 350 °C. After 4 h of annealing no significant changes occur in the Mössbauer spectrum anymore.

The rate of phase growth is determined by kinetic and thermodynamical parameters like the interdiffusivity constants ($\tilde{D}_a$ and $\tilde{D}_c$), interface reactions constants (K's) and equilibrium concentration (C's), which are functions of temperature. This can explain why the time derivative of the Mössbauer fraction of amorphous phase is different, for $T = 500$ °C, from the analog curve obtained for $T = 350$ °C. It is important to remember that not only the values of D's and K's are unequal for different temperatures, but also the C's because the curves of free energy (G_{Fe}, G_{Zr}, G_M, G_a, G_c in Fig. 7) have, at least, different positions for the two temperatures.[34]

Once again, we can not establish *a priori* if the other phase (amorphous) is growing, stopped, or shirinking away. It is only possible to say that the crystalline phase thickness grows more than the amorphous phase thickness [i.e., $(1/X)(dX/dt) > (1/X_A)(dX_A/dt)$]. It is clear that to obtain values from Eqs. (15)–(17) to the growing rates of the phase layer thickness, is necessary to know the diffusion parameters (J's, C's, and K's), which are not completely determined for the Fe-Zr multilayer system.

V. CONCLUSIONS

The solid-state reactions of $Fe_{0.33}Zr_{0.67}$ multilayers taken at 350 and 500 °C result in a formation of two phases: an amorphous phase and a crystalline phase corresponding to the intermetallic compound $FeZr_3$.

At first, the two phases (a-FeZr and c-$FeZr_3$) compete among themselves growing between the Fe and Zr layers until a new regime of diffusion is defined when the iron layer is exhausted. Then, the crystalline layer lies between an amorphous layer (with variable concentration) and a Zr layer.

At this stage the rate of reaction for both temperatures are diferent and also, may lead to a formation of amorphous phases with diverse stoichiometry formula. At 350 °C, the amorphous phase grows up until this includes 70% of the total number of Fe atoms. On the other hand, at 500 °C the crystal phase has grown until 68% of the Fe atoms are envolved.

Finally, we mention that as a function of the Fe concentration profile a model to the growing or shrinking of both phases was proposed. The rate of the growth of the amorphous-crystalline phases, expressed in terms of kinetic and thermodynamical parameters, is obtained in order to describe the experimental behavior of the $Fe_{0.33}Zr_{0.67}$ multilayered film.

ACKNOWLEDGMENTS

We thank Dr. A. Gomes and Dr. A. Vasquez for fruitful discussions. Thanks are also due to Dr. W. Schreiner for his help in the sample preparation.

[1] R. Schwarz and W. L. Johnson, Phys. Rev. Lett. **51**, 415 (1983).
[2] B. M. Clemens and M. J. Suchoski, Appl. Phys. Lett. **47**, 943 (1985).
[3] H. U. Krebs, D. J. Webb, and A. F. Marshall, Phys. Rev. B **35**, 5392 (1987).
[4] H. U. Krebs, D. J. Webb, and A. F. Marshall, J. Less-Common. Met. **140**, 17 (1988).
[5] H. U. Krebs, W. Biegel, A. Bienenstock, D. J. Webb, and T. H. Geballe, Mater. Sci. Eng. **97**, 163 (1988).
[6] H. U. Krebs, J. Less-Common Met. **145**, 97 (1988).
[7] D. E. Williamson and B. M. Clemens, Hyperfine Interact. **42**, 967 (1988).
[8] G. V. Kidson, J. Nucl. Mater. **3**, 21 (1961).
[9] B. E. Deal and A. S. Grove, J. Appl. Phys. **36**, 3770 (1965).
[10] C. Wagner, Acta Metall. **17**, 99 (1969).
[11] Ya. Ye. Geguzin and Yu. S. Kaganovskiy, Fiz. Metal. Metalloved. **39**, 553 (1975).
[12] H. H. Farrel, G. H. Gilmer, and M. Suenaga, Thin Solid Films **25**, 253 (1975).
[13] S. R. Shatynski, J. P. Hirth, and R. A. Rapp, Acta Metall. **24**, 1071 (1976).
[14] Ya. Ye. Geguzin, Yu. S. Kaganovskiy, L. M. Paritskaya, and V. I. Solunskiy, Phys. Met. Metall. **47**, 127 (1979).
[15] U. Gösele and K. N. Tu, J. Appl. Phys. **53**, 3252 (1982).
[16] V. I. Dybkov, J. Phys. Chem. Solids **47**, 735 (1986).
[17] U. Gösele and K. N. Tu, J. Appl. Phys. **66**, 2619 (1989).
[18] A. Paesano, Jr., S. R. Teixeira, and L. Amaral (to be published in Hyperfine Interact.).
[19] Fu-Rong Ding, P. R. Okamoto, and L. E. Rehn, Nucl. Instrum. Meth. B **39**, 122 (1989).
[20] F. Aubertin, U. Gonser, S. J. Campbell, and H.-G. Wagner, Z. Metallkde **76**, 237 (1985).
[21] T. O. Malakhova and Z. M. Alekseyeva, J. Less-Common Met. **81**, 293 (1981).
[22] M. Ghafari, U. Gonser, H.-G. Wagner, and M. Naka, Nucl. Instrum. Meth. **199**, 197 (1982).
[23] I. Vincze, F. Van der Woude, and M. G. Scott, Solid State Commun. **37**, 567 (1981).
[24] K. H. J. Buschow and P. H. Smit, J. Magn. Magn. Mater. **23**, 85 (1981).
[25] K. M. Unruh and C. L. Chien, Phys. Rev. B **30**, 4968 (1984).
[26] G. Le Caër, J. M. Cadogan, R. A. Brand, J. M. Dubois, and H. J. Güntherodt, J. Phys. F: Met. Phys. **14**, L73 (1984).
[27] M. Maurer, J. M. Friedt, and J. P. Sanchez, J. Phys. F: Met. Phys. **15**, 1449 (1985).
[28] S. M. Fries, C. L. Chien, J. Crummenauer, H.-G. Wagner, and U. Gonser, Hyperfine Interact. **27**, 405 (1986).
[29] C. Michaelsen, H. A. Wagner, and H. C. Freyhardt, J. Phys. F: Met. Phys. **16**, 109 (1986).
[30] M. Przybylski, K. Krop, T. Stobiecki, and L. Dargel-Sulir, Hyperfine Interact. **27**, 425 (1986).
[31] J. Balogh, L. Bottyán, I. Dézsi, K. Papp, F. Aubertin, S. M. Fries, and U. Gonser, Hyperfine Interact. **28**, 803 (1986).
[32] F. Aubertin, G. L. Whittle, S. J. Campbell, and U. Gonser, Phys. Status Solidi a **104**, 397 (1987).
[33] R. E. Reed-Hill, *Physical Metallurgy Principles*, 2nd ed (van Nostrand, New York, 1973), p. 524.
[34] W. L. Johnson, Prog. Mater. Sci. **30**, 81 (1986).